Temperature dependence and effect of series resistance on the electrical characteristics of a polycrystalline diamond metal-insulator-semiconductor diode

W. P. Kang, J. L. Davidson, Y. Gurbuz, and D. V. Kerns
Department of Applied and Engineering Sciences, Vanderbilt University, Nashville, Tennessee 37235

(Received 10 August 1994; accepted for publication 20 March 1995)

Temperature dependency and the series resistance effect on the electrical characteristics of a polycrystalline diamond-based (Au/Ti)/undoped-diamond/doped-diamond metal-insulator-semiconductor Schottky diode were investigated in a temperature range 25–300 °C. The current-voltage (I-V) characteristics of the device show rectifying behavior with the forward bias conduction limited by series resistance. Over the temperature range investigated, the I-V data confirmed that the conduction mechanism of the diode is controlled by thermionic field emission. Modifying the thermionic field emission equation to include the series resistance model allows the ideality factor and barrier height of the Schottky diode to be calculated. Temperature dependence of the ideality factor and apparent barrier height was determined. By extrapolating the forward saturation current data, the evaluated ideality factor was observed to decrease from 2.4 to 1.1 while the apparent barrier increased linearly from 0.68 to 1.02 eV in the temperature range from 25 to 300 °C. The Richardson plot, $\ln(I_0/T^2)$ vs $10^3/T$, has linear characteristics and indicates a true barrier height of 0.31 eV. Analysis of the temperature-dependent series resistor measurements indicates a boron doping activation energy of 0.104 eV in the p diamond. The capacitance-voltage-frequency measurement confirmed that the measured capacitance varies with applied bias and frequency due to the presence of the Schottky barrier, impurity level, and high series resistance. Capacitance-frequency measurement at zero bias indicated that the degrading capacitance at high frequency is primarily due to the high series resistance of the bulk polycrystalline diamond. © *1995 American Institute of Physics.*

I. INTRODUCTION

Recent advances in the growth of diamond films by plasma-enhanced chemical-vapor deposition (PECVD) have accelerated the development of diamond technology for electronic device applications. The PECVD method allows polycrystalline diamond to be grown on many different substrates more practically than homoepitaxial diamond films. Polycrystalline diamond has potential for many device applications utilizing device structures such as field-effect transistors, bipolar junction transistors, and Schottky diodes. Despite grain boundaries and defects of polycrystalline diamond film, electronic devices such as field-effect transistors and Schottky diodes have been demonstrated.[1–5] Although two recent works[6,7] have been presented on metal-insulator-semiconductor (MIS) Schottky barriers made of polycrystalline diamond on silicon substrates, little has been reported on the transport mechanisms and the temperature dependency of the electrical characteristics over a wide range of temperatures.

We have fabricated and characterized new MIS Schottky diodes using thin polycrystalline diamond layered structures grown directly on conducting (tungsten) substrates. The devices are fabricated in the form of metal (M)/undoped-diamond (I)/p-doped diamond (S) MIS Schottky diode configurations, with varying thicknesses of the undoped-diamond layers and different top metal contacts. Electrical characteristics of the devices were found to arise from thermionic emission, series resistance, and in some cases space-charge-limited current. The comparison of different diode types with various i-diamond thicknesses and metal contacts will be reported in a separate article. In this article we present the results of a systematic investigation on the transport mechanism, the series resistance effects, and the temperature dependence of the electrical properties of (Au/Ti)/undoped-diamond/doped-diamond MIS Schottky diodes made of polycrystalline diamond film. The current-voltage (I-V) measurements over the temperature range 25–300 °C were analyzed to examine the transport mechanisms in the MIS junction and to evaluate the dependence of the diode parameters with temperature. The capacitance-voltage-frequency (C-V-F) characteristics of the device have also been investigated.

II. EXPERIMENTAL METHODS

Polycrystalline diamond films were deposited on a tungsten substrate by PECVD. To facilitate uniform and high-density diamond nucleation on the supporting substrate, pre-deposition surface preparation of the substrate was performed by rubbing the surface of the substrate with a 0.1 μm diamond paste. The substrate was then ultrasonically cleaned in acetone, methanol, rinsed in de-ionized water, and dried with a nitrogen jet. The PECVD diamond films were deposited on the prepared surface of the substrate in a chamber containing a mixture of 99% hydrogen (H_2) and 1% methane (CH_4) gas, substrate temperature 850 °C, and a dynamically pumped pressure of 40 Torr. The plasma was sustained from a 2.45 GHz, 1.5 kW microwave source.

 0021-8979/95/78(2)/1101/7/$6.00

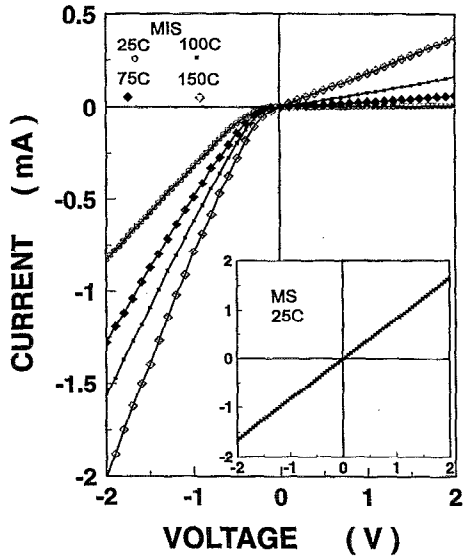

FIG. 1. Current-voltage characteristics of a (Au/Ti)/undoped-diamond/doped-diamond MIS Schottky diode at various temperatures. Insert: current-voltage characteristic of a (Au/Ti)/doped-diamond MS contact at 25 °C.

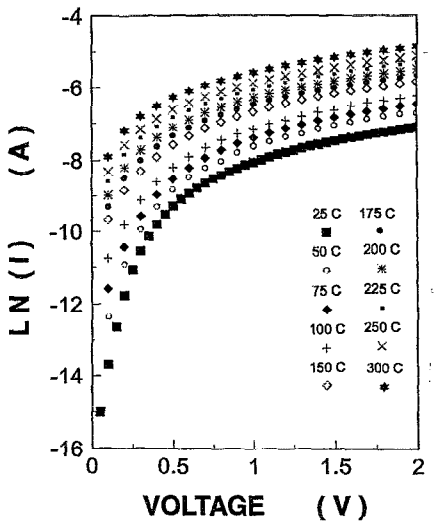

FIG. 2. Forward bias ln(I) vs V characteristics of a (Au/Ti)/undoped-diamond/doped-diamond MIS Schottky diode at various temperatures.

A p-type polycrystalline diamond film of 15 μm was deposited on the substrate. Boron doping was achieved via an *in situ* boron compound solid source doping method.[8] Subsequently a thin intrinsic (undoped) diamond layer 0.1 μm thick was selectively deposited on part of the p-diamond layer. The diamond films were then annealed for 1 min at 800 °C in an argon atmosphere using rapid thermal processing (RTP). The Raman spectra typical for diamond growth in this work shows the sp^3 peak at 1332 cm^{-1} and a low broad graphite peak at 1580 cm^{-1}. Au/Ti bilayer metal contacts 1 mm in diameter were deposited on the diamond surface of both the intrinsic (undoped) diamond and the p diamond in a vacuum of 10^{-6} Torr using the thermal evaporation technique to form (Au/Ti)/undoped-diamond/doped-diamond MIS Schottky diodes and (Au/Ti)/doped-diamond MS contacts, respectively.

I-V and C-V-F measurements were performed on the polycrystalline diamond MIS Schottky diode which was placed on a heating stage with a temperature range from 25 to 400 °C. The I-V measurements were conducted using a Hewlett Packard 4145B semiconductor parameter analyzer. A Hewlett Packard 4275A multifrequency *LCR* meter and a GenRad 1689M RLC Digibridge were used separately to perform C-V-F measurements. The C-V-F measurements were taken in parallel circuit mode with frequencies ranging from 500 Hz to 10 MHz. For all measurements, the tungsten ohmic contact to the p-diamond side was grounded and top metal (Au/Ti) contact voltages were swept from negative (forward bias) voltage to positive (reverse bias) voltage.

III. RESULTS AND DISCUSSIONS

A. Analysis of series resistance effects on I-V/T characteristics

I-V measurements of the MIS Schottky diode at different temperatures are shown in Fig. 1. The device shows rectification behavior; however, the forward and reverse leakage currents increased with increasing temperature, and the rectification ratio decreased as temperature increased. Nevertheless, rectifying behavior can be observed up to about 250 °C. For comparison, the I-V characteristic of a MS contact, a device without undoped-diamond interfacial layer, is shown in the insert of Fig. 1. The I-V characteristic is ohmic; thus, the presence of an undoped diamond interfacial layer for realization of the rectifying behavior is evident.

The current-voltage relationship for a MIS Schottky diode, based on the thermionic field emission model, is given by the following equations:[9,10]

$$I = I_0 \exp(qV/nkT)[1-\exp(-qV/kT)], \tag{1}$$

where I is measured current, V is voltage applied across the junction, q is the electronic charge, n is the ideality factor that describes departure from the ideal diode equation for reverse bias as well as forward bias, k is Boltzmann's constant, and T is device temperature (K). The prefactor I_0 is the extrapolated saturation current given by

$$I_0 = AA^{**}T^2 \exp(q\Phi_B/kT), \tag{2}$$

where A is the junction area, A^{**} is the effective Richardson constant, and Φ_B is the apparent barrier height. Under forward bias ($qV > 3kT$), Eq. (1) reduces to the familiar form often used to determine I_0,

$$I = I_0 \exp(qV/nkT). \tag{3}$$

A semilog plot of I vs V yields a linear relation where the intercept at $V=0$ is I_0 and the slope is q/nkT. Due to the high current under forward bias, these measurements are relatively immune to the effects of leakage paths. However, the high series resistance R_s of the diamond film limits the forward current and causes departures from linearity over much of the forward region, as evident in Fig. 2. Thus, accurate determination of I_0 and n cannot be obtained from the plot due to the effect of series resistance.

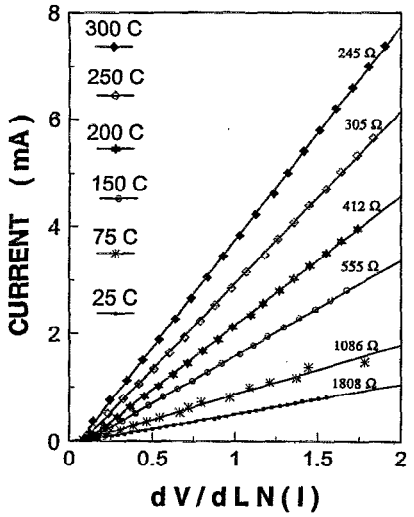

FIG. 3. Plots of I vs $dV/d\ \ln(I)$ of a MIS Schottky diode at various temperatures. The slope of a linear plot at a particular temperature indicates a constant series resistance value at that particular temperature.

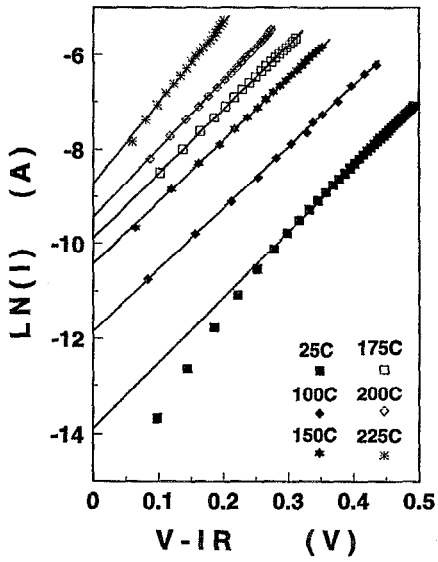

FIG. 4. Forward bias $\ln(I)$ vs $(V-IR)$ characteristics of a (Au/Ti)/undoped-diamond/doped-diamond MIS Schottky diode at various temperatures taking series resistances into consideration.

Series resistance has been observed to dominate current conduction processes in large-band-gap semiconductor materials[11] and has been reported to affect I-V measurements on diamond films by other research groups.[1,4,12] The series resistance contributes a prominent component because, at large currents, the voltage drop occurring across the series resistance of the diamond film is large and occurs in addition to the voltage drop across the junction. Therefore, the correct voltage across the junction is considered as $V-IR_s$, where R_s is the series resistance. Thus, the contribution of R_s to the experimental I-V data can be subtracted from the thermionic field emission model of Eq. (3) as

$$I=I_0 \exp[q(V-IR_s)/nkT]. \tag{4}$$

Differentiating Eq. (4), one gets the following equation:

$$I=\left(\frac{1}{R_s}\right)\left(\frac{dV}{d\ \ln(I)}\right)-\left(\frac{kT}{q}\right)\left(\frac{n}{R_s}\right). \tag{5}$$

The equation implies that if a plot of I vs $dV/d\ \ln(I)$ yields a straight line, then R_s can be obtained from 1/slope of that linear behavior. The I vs $d\ \ln(I)/dV$ characteristics of the MIS diode for different temperatures are shown in Fig. 3. The plots are indeed linear for the entire temperature range investigated. The slope of each curve provides the series resistance R_s value at that particular temperature. One can also obtain the series resistance of a Schottky diode from its forward bias I-V data using the approach described by Norde[13] or Lien, So, and Nicolet.[14]

Once the series resistance at a particular temperature has been evaluated by this method, its contribution to the experimental I-V data can be subtracted from Eq. (4). Figure 4 shows a family of $\ln(I)$ vs $(V-IR_s)$ plots for the entire temperature range investigated. The curves are linear over the entire voltage range. Accurate values of n and I_0 were then determined.

The prefactor I_0 can also be extracted from the reverse I-V characteristics through a semilog plot of $I/\{1-\exp[-q(V-IR_s)/kT]\}$ vs $(V-IR_s)$, obtained from Eq. (1) taking R_s into consideration. Figure 5 shows the I-V characteristics of the MIS Schottky diode at several temperatures plotted in this manner. I_0 is determined from the point where the curves cross the $V=0$ axis. Due to the low-current densities associated with reverse currents, the measurement is less effected by R_s. As is the case for extrapolation from semilog I-V characteristics in forward bias, the value of I_0 can be accurately determined from reverse bias semilog I-V since the plot is linear over the entire reverse region for the temperature range investigated. However, due to the heating effect caused by the reverse biasing of the junction, I_0 values obtained from the reverse bias region are slightly higher than those obtained from the forward bias region.

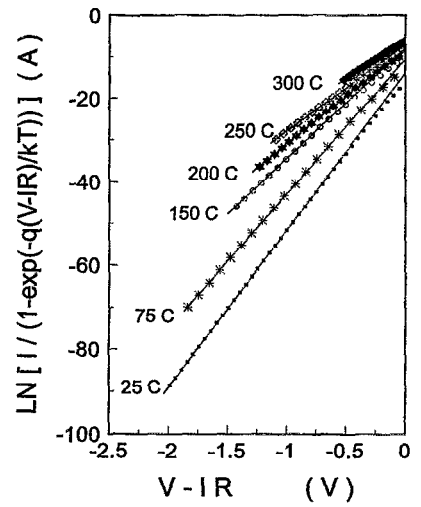

FIG. 5. Reverse bias $\ln(I/\{1-\exp[-q(V-IR)/kT]\})$ vs $(V-IR)$ characteristics of a (Au/Ti)/undoped-diamond/doped-diamond MIS Schottky diode at various temperatures taking series resistances into consideration.

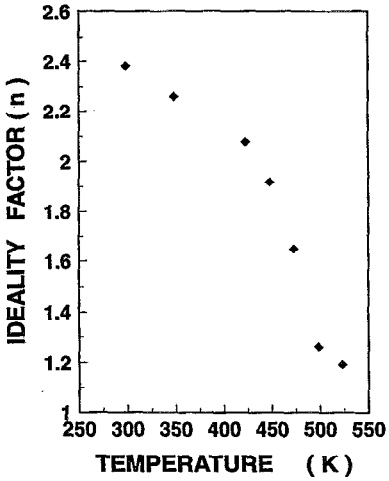

FIG. 6. Temperature dependence of ideality factor for a (Au/Ti)/undoped-diamond/doped-diamond MIS Schottky diode.

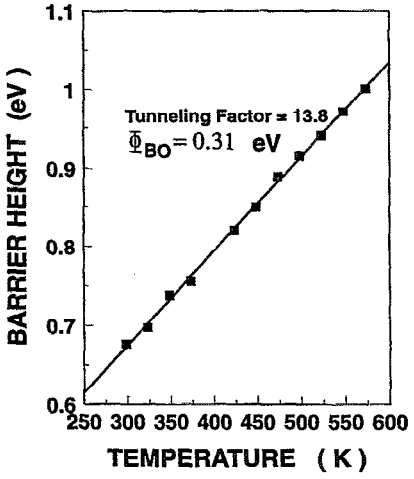

FIG. 7. Temperature dependence of apparent barrier height for a (Au/Ti)/undoped-diamond/doped-diamond MIS Schottky diode. The plot shows a linear relationship described by $q\Phi_B = q\Phi_{B0} + a\chi^{1/2}\delta kT$. The slope of the plot corresponds to the tunneling factor ($a\chi^{1/2}\delta$) of 13.8, and the intercept of the plot at $T=0$ K gives the $q\Phi_{B0}$ of 0.31 eV.

These examinations, therefore, indicate that the current conduction of the diode can be modeled by the modified thermionic field emission equation in both the forward bias and reverse bias regimes for the Schottky diode. The diode can be modeled as an Schottky barrier in series with R_s. From the corrected thermionic field emission model, accurate values of n and I_0 can be obtained.

B. Temperature dependence of device parameters

The ideality factor n, extracted from 1/slope of the $\ln(I)$ vs $(V-IR_s)$ plot of Fig. 4, is determined by

$$n=(q/kT)[d(\ln I)/d(V-IR_s)]^{-1}. \tag{6}$$

The temperature dependence of n is shown in Fig. 6. The ideality factor tends to decrease with increasing temperature. The range of the value n (2.4–1.1) and the temperature dependence behavior suggest a conduction mechanism controlled by the thermionic field emission. The high value of the ideality factor at low temperature is probably due to the potential drop in the interfacial layer and the recombination current through the interfacial states of the junction.

In the case of a MIS Schottky diode with an interfacial layer, Card and Rhoderick[10] reported that the extrapolated saturation current I_0 is given by

$$I_0 = AA^{**}T^2 \exp(-a\chi^{1/2}\delta)\exp(-q\Phi_{B0}/kT), \tag{7}$$

where A is the junction area, A^{**} is the effective Richardson constant, Φ_{B0} is the barrier height at zero bias, $a=(2/\hbar)(2m)^{1/2}$ is a constant that depends on the carrier effective mass m and Planck's constant $\hbar$, δ is the thickness of the interfacial film through which the carriers tunnel, and χ is the mean tunneling barrier presented by the interfacial layer. The term $a\chi^{1/2}\delta$ is collectively called the electron tunneling factor.

Therefore, from Eqs. (2) and (7), $q\Phi_B$ (apparent barrier height) is related to $q\Phi_{B0}$ (zero bias barrier height) through the relation

$$q\Phi_B = q\Phi_{B0} + a\chi^{1/2}\delta kT. \tag{8}$$

Thus, the apparent barrier height is a linear function of temperature.

The apparent barrier height $q\Phi_B$ can be determined from the extrapolated saturation experimental current I_0 in Fig. 4. From Eq. (2), $q\Phi_B$ is related to I_0 by

$$q\Phi_B = kT \ln(AA^{**}T^2/I_0). \tag{9}$$

Using an effective Richardson constant A^{**} of 120 $A/K^2\,cm^2$,[15] the temperature dependence of $q\Phi_B$ (apparent barrier height), evaluated for each I_0, is shown in Fig. 7. When the temperature increases the apparent barrier height increases. A linear temperature dependence of $q\Phi_B$ is observed as theoretically expected from Eq. (8). The slope of the plot corresponds to the tunneling factor ($a\chi^{1/2}\delta$) of 13.8, and the intercept of the plot at $T=0$ K gives the $q\Phi_{B0}$ of 0.31 eV. At room temperature, $q\Phi_B$ is 0.68 eV. However, because the theoretical value of χ is not available at this stage, a direct comparison between the experimental and theoretical values of tunneling factor would be useless.

In order to independently confirm the above findings, a Richardson plot $\ln(I_0/T^2)$ vs $10^3/T$ was taken for I-V curves measured at various temperatures. The principal advantage of determining Schottky barrier value by means of a Richardson plot is that no accurate knowledge of A and A^{**} values are required. This feature is particularly important in the investigation of a novel MIS interface. It is easy to interpret from Eq. (7) that

$$\ln(I_0/T^2) = -q\Phi_{B0}/kT + \ln(AA^{**}) - a\chi^{1/2}\delta. \tag{10}$$

Figure 8 shows the Richardson plot $\ln(I_0/T^2)$ vs $10^3/T$ for the MIS diode. A straight line is found as expected from the above equation. The barrier height Φ_{B0} determined from the slope of the straight line is 0.315 eV (this value agrees with the one, $\Phi_{B0}=0.31$ eV, obtained independently from Fig. 7). The extrapolated interception of the plot on the vertical axis gives the value of $\ln(AA^{**})-(a\chi^{1/2}\delta)$. Using the tunneling

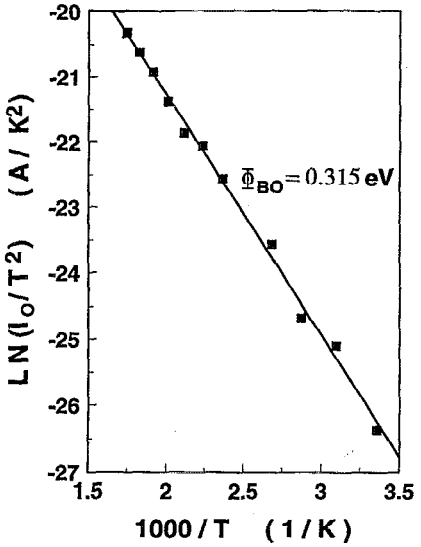

FIG. 8. Richardson plot of $\ln(I_0/T^2)$ vs $1/T$ for a (Au/Ti)/undoped-diamond/doped-diamond MIS Schottky diode.

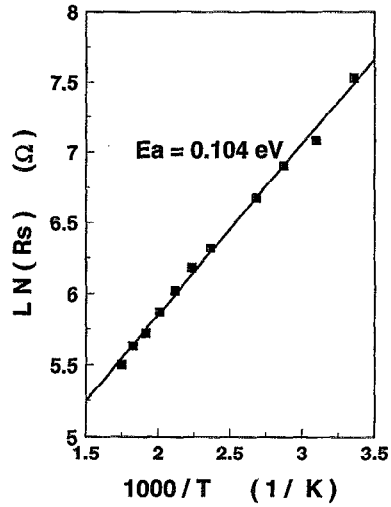

FIG. 9. Plot of $\ln(R_s)$ vs $1/T$ for a (Au/Ti)/undoped-diamond/doped-diamond MIS Schottky diode.

factor of 13.8 obtained in Fig. 7 and the area A of 7.85×10^{-3} cm^{-2}, the value of A^{**} obtained experimentally from the Richardson plot is about 110 $A/K^2\,cm^2$ which is in good agreement with the theoretical value.[15] However, it is believed that the transmission of carriers through the interfacial layer cannot be due solely to simple tunneling. Some other process must also be involved, perhaps trap-assisted tunnelling through the interfacial layer.

Analysis of the I-V/T data, in the previous section, has confirmed that the forward branch of the I-V characteristic is dominated by the bulk resistance of the diamond. The temperature dependence of the bulk resistance is inversely related to bulk conductivity σ which can be described by the equation[15]

$$1/R_s \propto \sigma = \text{const}\exp(-E_A/kT). \tag{11}$$

Thus, a plot of $\ln(R_s)$ vs $1/T$ should be linear and the slope corresponds to the activation energy E_A. The plot shown in Fig. 9 is indeed linear, and the activation energy is 0.104 eV (above the valence band) which implies the presence of acceptor impurities. For boron-doped CVD diamond, the activation energy has been found to be a strong function of the deposition conditions and the doping level, varying between 0.013 and 0.37 eV.[16] The activation energy E_A determined here falls in this range of reported values. Since the reported activation energy for undoped polycrystalline diamond is close to 1 eV,[17,18] this evaluated E_A of 0.104 eV indicates that the series resistance arises from the boron-doped layer of the MIS Schottky diode.

C. Effects of series resistance on *C-V-F* measurements

C-V-F measurements were performed on the MIS Schottky diode in the reverse bias region. Figure 10 shows the *C-V-F* response for the Schottky diode, indicating that the measured capacitance is dependent on the reverse bias voltage and frequency. The voltage and frequency dependence is due to the factors of a Schottky barrier, boron-doped impurity levels, and high series resistance. At low frequency the measured capacitance is dominated by the depletion capacitance of the diamond Schottky diode which is bias dependent and frequency independent. As the frequency is increased, the total diode capacitance is affected not only by the depletion capacitance but also by the bulk diamond resistance and the dispersion capacitance, which is frequency dependent and associated with hole emission from slowly responding deep impurity levels.[9,19] Because of these effects, the capacitance-bias dependence becomes less pronounced or disappears. Similarly, the frequency dependence is weakened for high reverse voltages. Similar results have been observed on bulk diamond and single-crystal diamond[16,20,21] Schottky diodes.

Theoretical description of the *C-V-F* dependency for a synthetic-diamond-based Schottky diode, taking series resistance of the bulk into consideration, has been developed by

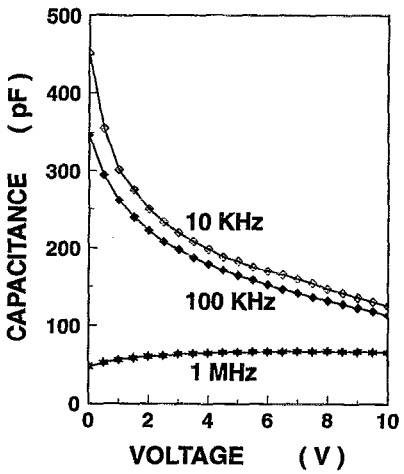

FIG. 10. Reverse bias *C-V-F* characteristics of a (Au/Ti)/undoped-diamond/doped-diamond MIS Schottky diode.

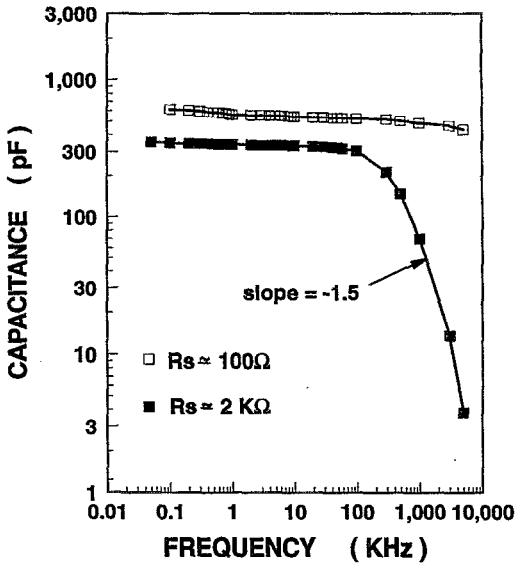

FIG. 11. Zero bias C-F plots of two (Au/Ti)/undoped-diamond/doped-diamond MIS Schottky diodes with two different series resistance values of 100 Ω and 2 kΩ.

Glover.[20] It was found that the junction capacitance could be represented by a series equivalent circuit consisting of capacitors C_d and C_f and resistance R_f and R_s, described by the following equations:[20]

$$C_m(V,\omega,T)=C_T/[1+(\omega R_T C_T)^2], \tag{12}$$

where $1/C_T=1/C_d(V)+1/C_f(\omega,T)$, and $R_T=R_f(\omega,T)+R_s(T)$. C_m is the measured capacitance, C_d is the depletion capacitance which is voltage dependent, but frequency and temperature independent. C_f (which is proportional to $\omega^{-1/2}$) is the capacitance due to the additional junction length required at higher frequencies for hole emission from the slowly responding deep levels. The dissipative loss due to the phase shift is represented by R_f, and R_s is the series resistance of the bulk diamond. In the case of the MIS Schottky diode studied here, a slightly modified term in

$$1/C_T=1/C_0+1/C_d(V)+1/C_f(\omega,T)$$

is needed to account for the contribution of the capacitance C_0 by the i-diamond layer. According to this model, Glover[20] concluded that at high frequencies or low temperature $C_I \rightarrow C_f$. One can then distinguish two cases, depending on the value of R_s. When $R_s=0$, $\omega C_T R_T=1$ so that $C_m=C_f/2$, and the measured capacity falls off with frequency as $\omega^{-1/2}$. When $R_s \gg R_f$, however, the second term in the denominator of Eq. (12) dominates, so that C_m depends on frequency as $\omega^{-3/2}$. Figure 11 confirms these limiting cases of the series resistance effects on the C-F characteristics of the MIS diode at room temperature. The figure shows two individual plots of measured capacitance versus frequency at zero bias for two MIS Schottky diodes with different series resistance values of 100 Ω and 2 kΩ. At high frequencies (>100 kHz) the capacitance of the diode with high series resistance begins to decline with a slope of −1.5 (i.e., showing $C_M \alpha$ frequency$^{-3/2}$). This slope is due to the high series resistance of the device. For the Schottky diode with a small series resistance, $R_s=100$ Ω, the capacitance versus frequency plot for this device shows a slope of −0.5, which is much smaller than the slope for the Schottky diode with high series resistance (slope=−1.5). The characteristic slopes of −1.5 (for a device with high series resistance) and −0.5 (for device with low series resistance) at high frequency are in agreement with the theoretical work described by Glover[20] on synthetic crystalline diamond. Our experimental data have confirmed the characteristic features of this dependence.

IV. CONCLUSIONS

The temperature dependence and series resistance effects on the electrical parameters of a new (Au/Ti)/undoped-diamond/doped-diamond MIS Schottky diode have been characterized and analyzed. The (Au/Ti)/undoped-diamond/doped-diamond structures show rectifying behavior. An interfacial i-diamond layer is found to be a means for fabricating diamond-based MIS diodes with satisfactory low leakage currents for high-temperature operation. The conduction mechanisms of the polycrystalline diamond Schottky diodes investigated were controlled by thermionic field emission. The modified thermionic field equation using a series resistance model allows the ideality factor and barrier height of the diode to be calculated. The barrier heights were calculated by means of two factors, the modified semilog I-V characteristics at several temperatures and the Richardson plot. The Richardson plot is linear, indicating that the experimental Richardson plot is reliable. The calculated barrier height varies linearly with temperature and the ideality factor decreases with temperature. Semilog I vs V is linear for both the forward and reverse bias regions, over the entire temperature range studied in this work. The values of n calculated from the linear region are 2.4–1.1 indicating that the (Au/Ti)/undoped-diamond/doped-diamond MIS diode does obey the thermionic field emission model. C-V-F measurements confirmed that the measured capacitance varies with applied bias and frequency. This dependence is due to the presence of the Schottky barrier, boron doping, and series resistance. At high frequencies, devices with high series resistance had declining capacitance with increasing frequency. Determination of the barrier height using $1/C^2$-V plot was not possible due to high series resistance effects at high frequency and the voltage intercept is offset by the i-diamond layer capacitance at low frequency. It is clear that ignoring the series resistance R_s can lead to significant errors in the analysis of the C-V-F characteristics.

[1] K. Nishimura, K. Das, and J. T. Glass, J. Appl. Phys. **69**, 3142 (1991).
[2] A. J. Tessmer, L. S. Plano, and D. L. Dreifus, IEEE Electron Device Lett. **EDL-14**, 66 (1993).
[3] G. Sh. Gildenblat, S. A. Grot, C. W. Hatfield, A. R. Badzian, and T. Badzian, IEEE Electron Device Lett. **EDL-11**, 371 (1990).
[4] G. Zhao, E. M. Charlson, E. J. Charlson, T. Stacy, J. M. Meese, G. Popovici, and M. Prelas, J. Appl. Phys. **73**, 1832 (1993).
[5] C. Gomez-Yanez and M. Alam, J. Appl. Phys. **71**, 2303 (1992).
[6] K. Miyata, D. L. Dreifus, and K. Kobashi, Appl. Phys. Lett. **60**, 480 (1992).
[7] V. Venkatesan, K. Das, G. G. Fountain, R. A. Rudden, J. B. Posthill, and R. J. Markunas, J. Electrochem. Soc. **139**, 1445 (1992).

[8] L. M. Edwards, Ph. D. thesis, Vanderbilt University, 1992.
[9] E. H. Rhoderick and R. H. Williams, *Metal-Semiconductor Contacts* (Clarendon, Oxford, 1988).
[10] H. C. Card and E. H. Rhoderick, J. Phys. D **4**, 1589 (1971).
[11] D. E. Heller, R. M. Dawson, C. T. Malone, S. Nag, and C. R. Wronski, J. Appl. Phys. **72**, 2377 (1992).
[12] B. Huang, D. K. Reinhard, and J. Asmussen, Diamond Related Mater. **2**, 812 (1993).
[13] H. Norde, J. Appl. Phys. **50**, 5052 (1979).
[14] C. D. Lien, F. C. T. So, and M.-A. Nicolet, IEEE Trans. Electron Devices **ED-31**, 1502 (1984).
[15] S. M. Sze, *Physics of Semiconductor Devices* (Wiley, New York, 1981).
[16] G. Sh. Gildenblat, S. A. Grot, C. R. Wronski, M. C. Hicks, A. R. Badzian, T. Badzian, and R. Messier, in *Proceedings of IEDM*, 1988, pp. 626–629.
[17] Y. Muto, T. Sugino, J. Shirafjui, and K. Kobashi, Appl. Phys. Lett. **59**, 843 (1991).
[18] J. A. von Windheim, V. Venkatesan, D. M. Malta, and K. Das, Diamond Related Mater. **2**, 841 (1993).
[19] C. R. Crowell and K. Nakano, Solid-State Electron. **15**, 605 (1972).
[20] G. H. Glover, Solid-State Electron. **16**, 973 (1973).
[21] V. Venkatesan, K. Das, J. A. von Windheim, and M. W. Geis, Appl. Phys. Lett. **63**, 1065 (1993).